Photoelectrocatalytic reduction of CO_2 to methanol over the multi-functionalized TiO_2 photocathodes

Yanjie Xu [a], Yongjian Jia [a], Yuqian Zhang [a], Rong Nie [a], Zhenping Zhu [b], Jianguo Wang [b], Huanwang Jing [a,b,*]

[a] State Key Laboratory of Applied Organic Chemistry, College of Chemistry and Chemical Engineering, Lanzhou University, Lanzhou 730000, PR China
[b] State Key Laboratory of Coal Conversion, Institute of Coal Chemistry, Chinese Academy of Sciences, Taiyuan 030001, PR China

ARTICLE INFO

ABSTRACT

The photoelectrocatalytic (PEC) reduction of CO_2 to chemical fuels was achieved by utilizing the multi-functionalized TiO_2 film photocathodes. On the surfaces of TiO_2 films, Pd nanoparticles were introduced to catch protons, molecules of Eosin Y disodium salt were embedded to absorb solar energy, and four different amine ligands were immobilized to capture and activate CO_2. In the novel PEC cells, multi-functionalized TiO_2 and Co-Pi/W:$BiVO_4$ films were served as photocathode and the counter electrode, respectively. It was found that methanol was the major liquid product. Besides, some ethanol and acetone can be detected as well. The maximum formation rate and the highest selectivity of methanol were $43.6 \, \mu M \, cm^{-2} \, h^{-1}$ and approximately 100%, respectively. The Faradaic efficiencies of the PEC cells can exceed 1000% with the aid of photoelectrons. The $^{13}CO_2$ labeling experiments verify that methanol and carbon monoxide are derived from CO_2.

© 2016 Elsevier B.V. All rights reserved.

1. Introduction

The increasing consumption of fossil fuels accompanying with large amounts of CO_2 emission, have resulted in energy crisis and global warming [1]. Therefore, the CO_2 fixation and conversion attracted increasing attentions in recent years [2–6]. The photocatalytic and electrocatalytic reduction of CO_2 to chemical fuels, such as ethanol, methanol and acetone, provided promising solutions [7–12]. As an n-type semiconductor, TiO_2 was firstly applied in the water splitting by Honda et al. in 1972 [13]. Subsequently, they further reported that the PEC reduction of CO_2 with TiO_2 in water could produce small amounts of methanol, formic acid, formaldehyde and methane [14]. Since then, TiO_2 was intensively investigated as an ideal photocatalyst owing to its low cost, superb stability, environmentally friendly and nontoxic properties [13–16].

However, it is well-known that only ultraviolet light can be absorbed because of the wide bandgap (3.0–3.2 eV) of anatase and rutile TiO_2 [17,18]. Hence, it is necessary to ameliorate the photocatalysis efficiency of TiO_2. It was reported that dyes and quantum dots could be utilized to enlarge the light-harvesting abilities of semiconductors [9,15,19–21]. Besides, the charge-hole separation efficiency of semiconductors can be improved by metal loading and various nanocomposite designs [22–27]. Notably, these methods have been used in the CO_2 reduction application as well [28–31].

Nowadays, photocatalysis, electrocatalysis and photoelectrocatalysis are three common methods for CO_2 reduction in water [9,32]. In comparison with photocatalysis systems, photoelectrocatalytic (PEC) cells have more advantages because the external voltage could prevent photoelectron-hole pairs from recombination during the CO_2 reduction process [9]. Although electrocatalysis systems contribute to the transfer of proton and electron, electrodes commonly suffer from high over potential that induces large H_2 releasing and low selectivity for carbon-based molecules [33,34]. Moreover, the surfaces of photoelectrodes can evidently affect the conversion efficiency of PEC cells [35–38]. Additionally, an appropriate modification of electrodes could provide adsorption sites for CO_2 [9,39]. Consequently, the PEC efficiency of TiO_2 for CO_2 reduction can be enhanced by chemical modifications of electrodes. However, their conversion efficiencies of CO_2 are still rather low and cannot satisfy the requirement for industrial applications.

In this study, the surfaces of TiO_2 electrodes were functionalized by amine ligands, Pd nanoparticles and Eosin Y disodium salt (EY), in turn. The PEC reduction of CO_2 was performed in a three-electrode PEC system under simulated sunlight with appropriate external potential in $KHCO_3$ aqueous solution. The experiment

* Corresponding author at: State Key Laboratory of Applied Organic Chemistry, College of Chemistry and Chemical Engineering, Lanzhou University, Lanzhou 730000, PR China.
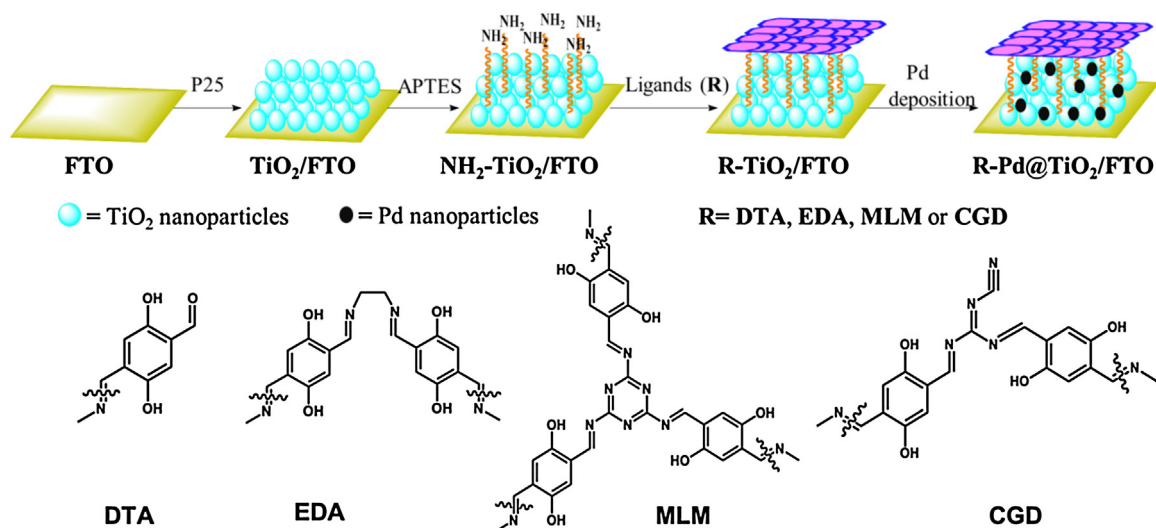*E-mail address:* hwjing@lzu.edu.cn (H. Jing).

Fig. 1. Schematic diagrams of the preparation processes of multi-functionalized TiO_2 photocathodes and the structures of different organic ligands.

results revealed that the light-harvesting ability of TiO_2 and the conversion rate of CO_2 were both improved remarkably. The related mechanisms were discussed in detail.

2. Experimental section

2.1. Fabrication procedures of multi-functionalized electrodes

Fluorine-tinoxide (FTO) glasses and TiO_2-P25 powder (P25) were purchased from Nippon Sheet Glass, Germany Degussa, respectively. The preparation procedures of TiO_2/FTO electrodes are illustrated in Fig. 1. The synthesis procedures of 2,5-dihydroxy-terephthalaldehyde (DTA) and the fabrication processes of tungsten-doped and Co-Pi modified $BiVO_4$ (Co-Pi/W:$BiVO_4$) electrode are available in Supplementary material.

2.1.1. Preparation of TiO_2/FTO film electrodes

The TiO_2/FTO electrodes were prepared by spreading P25 aqueous slurry on FTO substrate using vacuum spincoater. The slurry was obtained by grinding a mixture of 4 g P25, 200 μL Triton X-100, 8 mL deionized water and 500 mg polyethylene glycol (molecular weight 20000) according to the previous report [40]. The fabricated TiO_2/FTO electrodes were sintered at 450 °C for 1 h in a muffle furnace.

2.1.2. Surface modification of TiO_2/FTO film electrodes with organic ligands

As shown in Fig. 1, the NH_2-TiO_2/FTO electrodes can be obtained by immersing TiO_2/FTO electrodes into a solution followed by holding at 70 °C for 6 h, where the solution contained 30 mL ethanol, 1.5 mL 3-aminopropyl-triethoxysilane (APTES) and 1 mL deionized water. To get DTA-TiO_2/FTO electrodes, the dried NH_2-TiO_2/FTO electrodes were soaked in 30 mL THF solution with 50 mg 2,5-dihydroxyterephthalaldehyde (DTA) and refluxed for 6 h. Then, the DTA-TiO_2/FTO electrodes were refluxed for 6 h in 30 mL THF solutions with 10 mmol ethyl diamine (EDA), melamine (MLM) or 2-cyanoguanidine (CGD), respectively. Subsequently, four different functionalized TiO_2 electrodes with net-like structures can be successfully fabricated when the obtained electrodes in the previous step were refluxed for 6 h in 30 mL THF solution containing 1 mL salicylaldehyde. The four functionalized TiO_2 electrodes with different organic ligands (R) were designated as DTA-TiO_2, EDA-TiO_2,
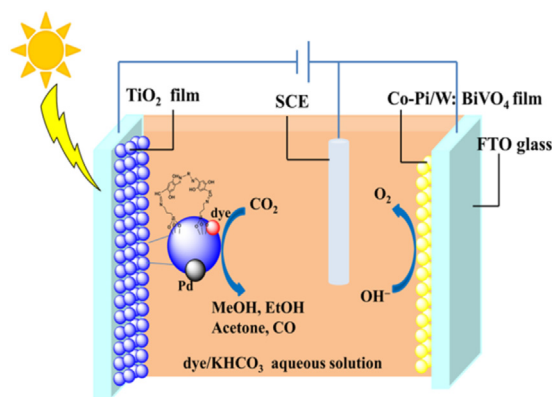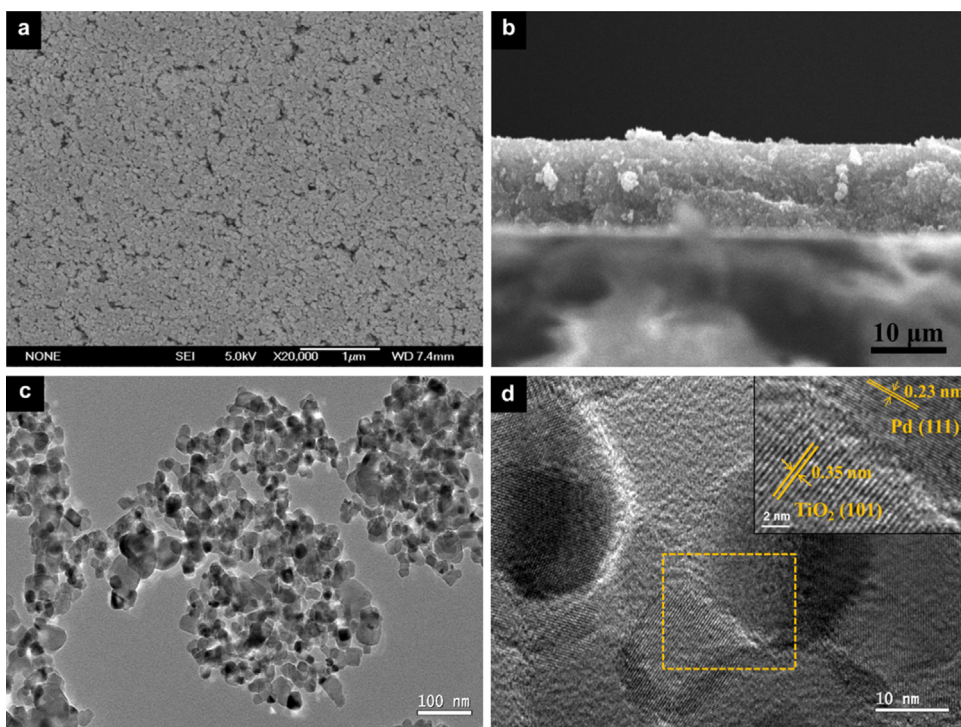
MLM-TiO_2, and CGD-TiO_2, respectively. The structures of different organic ligands (R) were illustrated in Fig. 1.

2.1.3. Metal deposition and dyes adsorption

Pd nanoparticles were deposited onto the TiO_2 films to obtained R-Pd@TiO_2 electrodes by pulse electrodeposition technique [41]. When R-Pd@TiO_2 electrodes were immerged into the electrolytes containing EY, the dye-R-Pd@TiO_2 electrodes could be obtained immediately. It is worth mentioning that both TiO_2 and $BiVO_4$ electrodes were rinsed with deionized water and dried at 70 °C in vaccum before use.

2.2. Photoelectrochemical measurement

The linear sweep voltammetry (LSV) and amperometric i-t curves were measured in a three-electrode system using an electrochemical workstation. In the new PEC cells, dye-R-Pd@TiO_2 electrode was served as the photocathode, the Co-Pi/W:$BiVO_4$ film was employed as the counter electrode and a saturated calomel electrode (SCE) was used as the reference electrode (Fig. 2). The PEC reduction of CO_2 was performed in the $KHCO_3$ aqueous solution (0.1 M, 60 mL) under simulated sunlight irradiation and appropriate external potential. The electrolyte containing EY (1 mM) was saturated with CO_2 (99.998%) or Ar for 30 min prior to photoelectrochemical measurements. The pH of CO_2-saturated electrolyte was about 6.7. The simulated sunlight source was a 300 W Xenon

Fig. 2. Schematic plots of the new PEC cell for CO_2 reduction.

Fig. 3. Microscopy images of EDA-Pd@TiO$_2$ film electrode: (a) SEM image of surface morphology; (b) cross-sectional SEM image; (c) bright-field TEM image and (d) corresponding HRTEM image.

lamp (PLS-SXE300/300UV). The intensity of the light source was adjusted to 100 mW/cm^2 calibrated by a standard silicon cell. The external potential was provided by an electrochemical workstation (CHI660E).
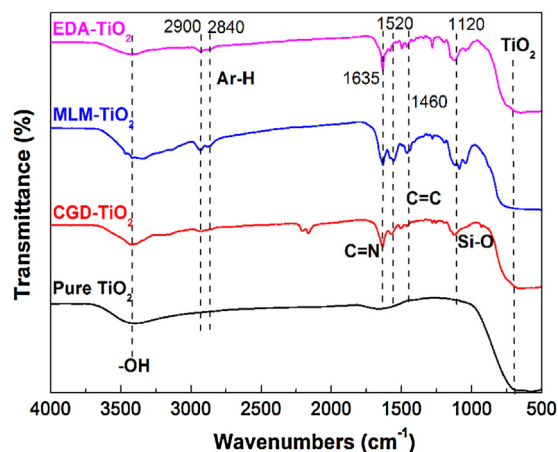
2.3. Characterizations

The solid-state UV–vis absorption spectra were conducted on a UV–vis spectrophotometer (UV-2600, Shimadzu). A JSM-6701F field-emission scanning electron microscope (FESEM) was used to observe the morphology of TiO$_2$ film. A FEI Tecnai G2 TF30 field emission transmission electron microscope (TEM) with an accelerating voltage of 300 kV was employed to observe the morphologies of TiO$_2$ as well. Fourier transform infrared (FT-IR) spectra were recorded on a Nicolet NEXUS 670 instrument. X-ray photoelectron spectra (XPS) were collected by a Kratos AXIS Nova spectrometer (Shimazu Co., Ltd.) with a monochro-matic Al Kα X-ray. ^{1}H nuclear magnetic resonance (^{1}H NMR, JNM-ECS 400 MHz, JOEL) spectrum was utilized to analyze the liquid products with dimethylsulfox-ide (DMSO, 10 mM) and *m*-trihydroxybenzene (MTB, 50 mM) as internal standards. Gas chromatography (GC, VARIAV CP-3380) and gas chromatography-mass spectrometer (GC–MS, Agilent 7890A-Agilent 5975C) were employed to detect gas-phase products.

3. Results and discussion

3.1. Characterization of photocathodes

The prepared dye-R-Pd@TiO$_2$ photocathodes were examined by various techniques. As shown in Fig. 3, TiO$_2$ nanoparticles in EDA-Pd@TiO$_2$ electrode were closely stacked on the FTO substrate and the thickness of TiO$_2$ film was about 15 μm. The main elements distribution on the surface was depicted in Fig. S1c, in which, Pd nanoparticles were uniformly deposited on TiO$_2$ film electrode. The TEM image of the EDA-Pd@TiO$_2$ film was shown in Fig. 3c. The

Fig. 4. FT-IR spectra of pure TiO$_2$ and organic ligands functionalized TiO$_2$ electrodes.

corresponding HRTEM image (Fig. 3d) verified that the Pd nanoparticles were modified on the TiO$_2$ successfully. It can be seen from XRD patterns (Figs. S3 and S4) that TiO$_2$ and BiVO$_4$ in electrodes are anatase and clinobisvanite structures, respectively.

The modification of organic ligands on TiO$_2$ surfaces was confirmed by FT-IR spectra. As shown in Figs. 4 and S5, the peaks at 2900 and 2840 cm^{-1} were assigned to Ar—H and C—H. The peak at 1635 cm^{-1} corresponded to the typical stretching vibration modes of C=N [27]. The peaks at 1520 and 1460 cm^{-1} were attributed to the asymmetric breath vibration of Ar-rings. Moreover, the peak at 1120 cm^{-1} certified the existence of Si—O groups. Additionally, the thermo gravimetric analysis (Fig. S6) verified that the TiO$_2$ electrodes were successfully modified with organic ligands.

XPS analysis of EDA-Pd@TiO$_2$ was shown in Figs. 5 and S7. The peaks at 340.5 eV and 335.2 eV were assigned to 3d orbital of Pd$^{(0)}$
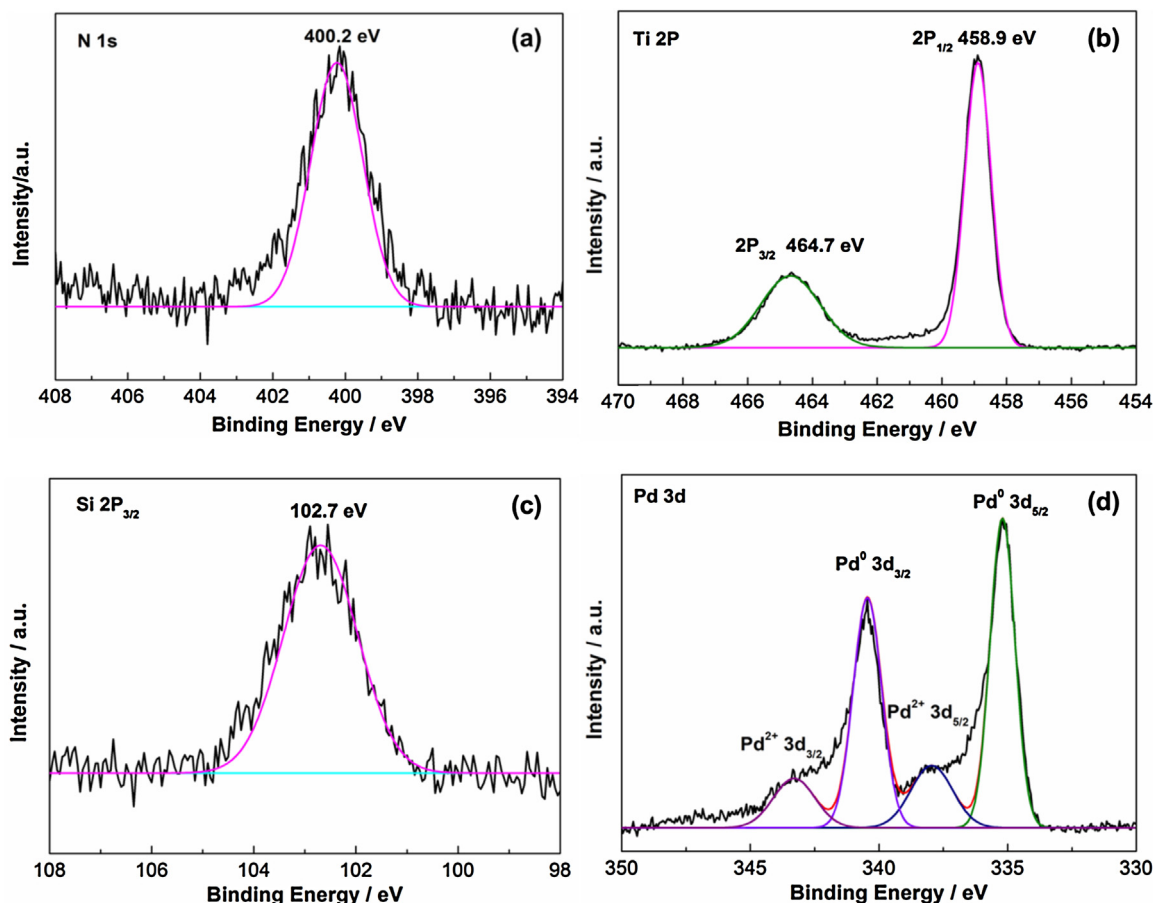
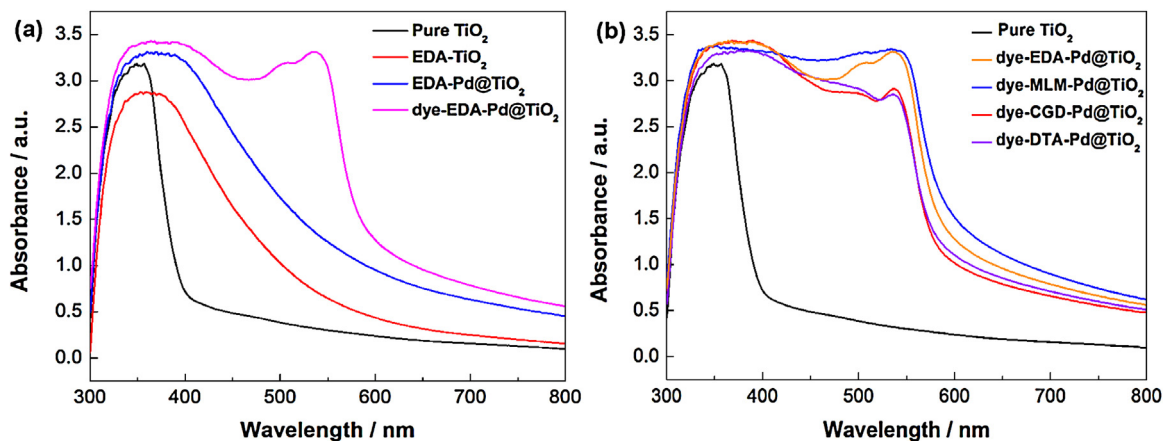**Fig. 5.** XPS spectra of (a) N 1s; (b) Ti 2P; (c) Si 2P and (d) Pd 3d in EDA-Pd@TiO$_2$ electrode.

Fig. 6. Solid-state UV–vis absorption spectra of (a) pure TiO$_2$, EDA-TiO$_2$, EDA-Pd@TiO$_2$ and dye-EDA-Pd@TiO$_2$ electrodes, (b) pure TiO$_2$, dye-EDA-Pd@TiO$_2$, dye-MLM-Pd@TiO$_2$, dye-CGD-Pd@TiO$_2$ and dye-DTA-Pd @TiO$_2$ electrodes.

atoms [42], which revealed the Pd nanoparticles were deposited on the surface of electrode successfully. The peaks of N 1s and Si 2p can be detected as well, indicating that amine ligands were successfully modified onto the surface of TiO$_2$ electrode.

The solid-state UV–vis absorption spectra of dye-R-Pd@TiO$_2$ electrodes were plotted in Figs. 6 and S8. Compared with pure TiO$_2$, the absorbance of EDA-TiO$_2$ was evidently improved in the visible light range (Fig. 6a). When Pd nanoparticles were deposited, the

absorbance was greatly enhanced on account of the surface plasmon resonance [43]. Furthermore, a strong absorbance appeared in the region of 500–600 nm after the dye was further adsorbed. The UV–vis spectra of four different TiO$_2$ electrodes were plotted in Fig. 6b. It follows that the light-harvesting abilities of dye-R-Pd@TiO$_2$ electrodes were dramatically enhanced in comparison with pure TiO$_2$.
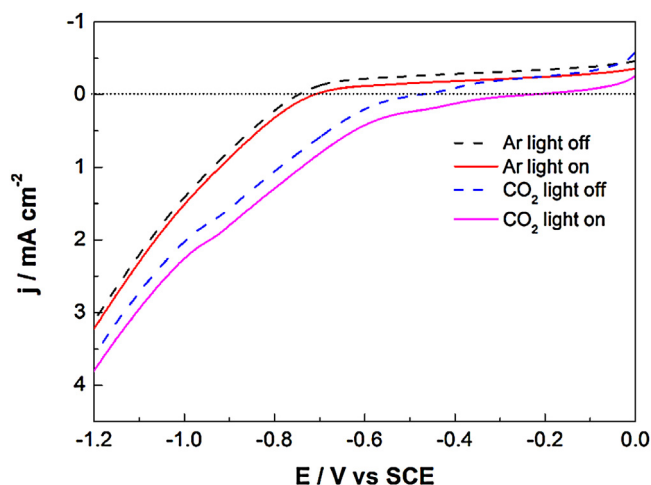
Fig. 7. LSV curves of dye-EDA-Pd@TiO$_2$ photocathode in 0.1 M KHCO$_3$ aqueous solution with Ar or CO$_2$ saturated.

3.2. Photoelectrocatalytic properties

The LSV experiments were conducted in 0.1 M KHCO$_3$ aqueous solutions with Ar or CO$_2$ saturated at a scan rate of 100 mV s^{-1} under simulated sunlight irradiation or dark. The LSV curves of dye-EDA-Pd@TiO$_2$ photocathode in Ar or CO$_2$ (Fig. 7) implied that, under the bias voltage of −0.5 V to −1.2 V (vs SCE), the photocurrent densities of PEC cells under CO$_2$ atmosphere were obviously

larger than under Ar atmosphere. It suggested that PEC reduction of CO$_2$ took place on the photocathodes and light irradiation played an important role in CO$_2$ reduction. The LSV curves of dye-MLM-Pd@TiO$_2$, dye-CGD-Pd@TiO$_2$ and dye-DTA-Pd@TiO$_2$ photocathode were measured as well, and shown in Fig. S9. Furthermore, the stability of EDA-Pd@TiO$_2$ photocathode was examined by cyclic voltammetry and long-term amperometric i-t measurement. As shown in Fig. S10, the current density was slightly fluctuated after 100 cycles of cyclic voltammetry. The photocurrent density of the PEC cell seldom decreased during 6 h irradiation (Fig. S11). It revealed that the multi-functionalized TiO$_2$ photocathodes were quite stable.

3.3. Photoelectrocatalytic reduction of CO$_2$

Here, considering the competition between hydrogen evolution reaction and CO$_2$ reduction reaction, the applied bias potential of cells were set as −0.5 V, −0.6 V, −0.7 V and −0.8 V (vs SCE), respectively. ^{1}H NMR with water suppression was employed to identify and quantify the liquid products with DMSO and MTB as internal standards [44]. When the CO$_2$ reduction reaction finished, it was found that methanol was the major liquid product and some ethanol and acetone were also detected according to the ^{1}H NMR analysis. Besides, CO and H$_2$ can be examined as well in the generated gas-phase by GC technique.

Figs. 8 and 9 illustrated the formation rates and selectivity of different reduction products. Besides, the detailed data was summarized and listed in Tables S1 and S2. As shown in Fig. 8a and Table S1, the Faradaic efficiencies of the cells under differ-
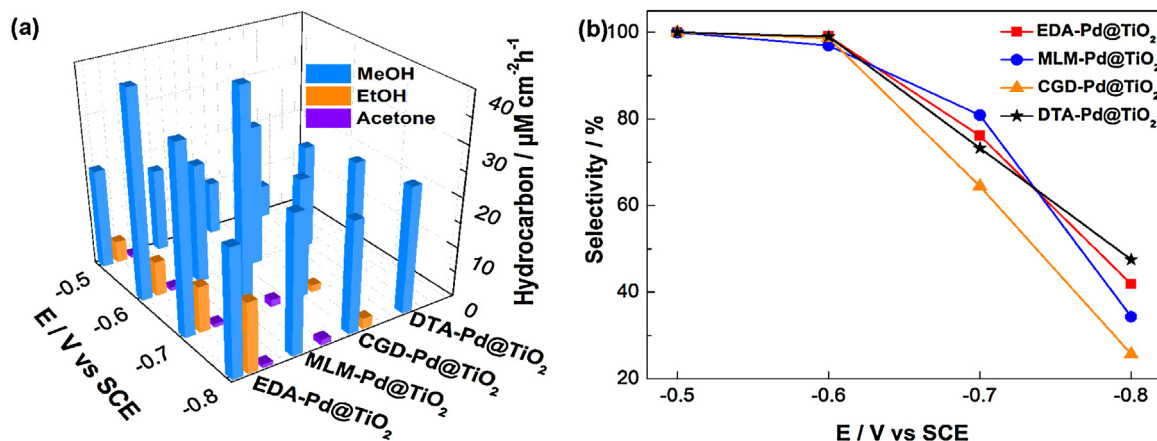

Fig. 8. (a) The formation rates of liquid products and (b) the selectivity of carbon-based products for four kinds of TiO$_2$ photocathode.
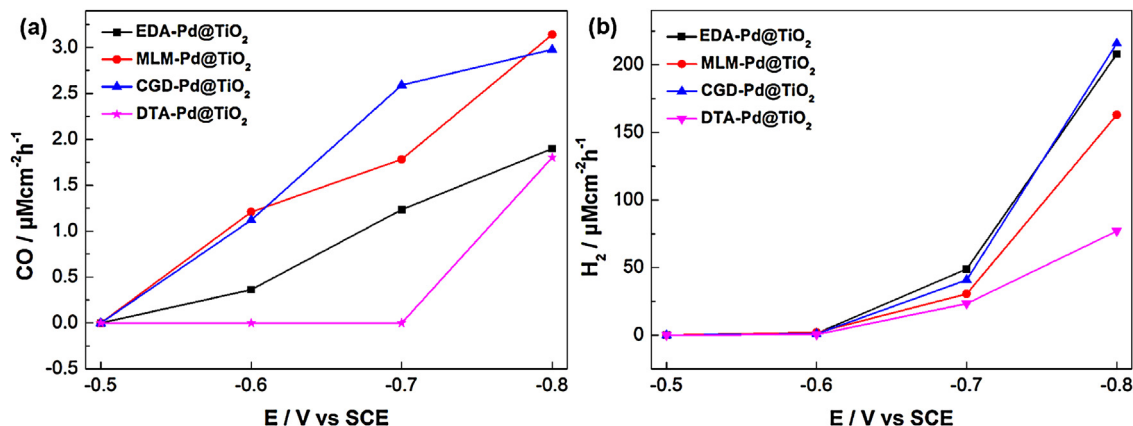

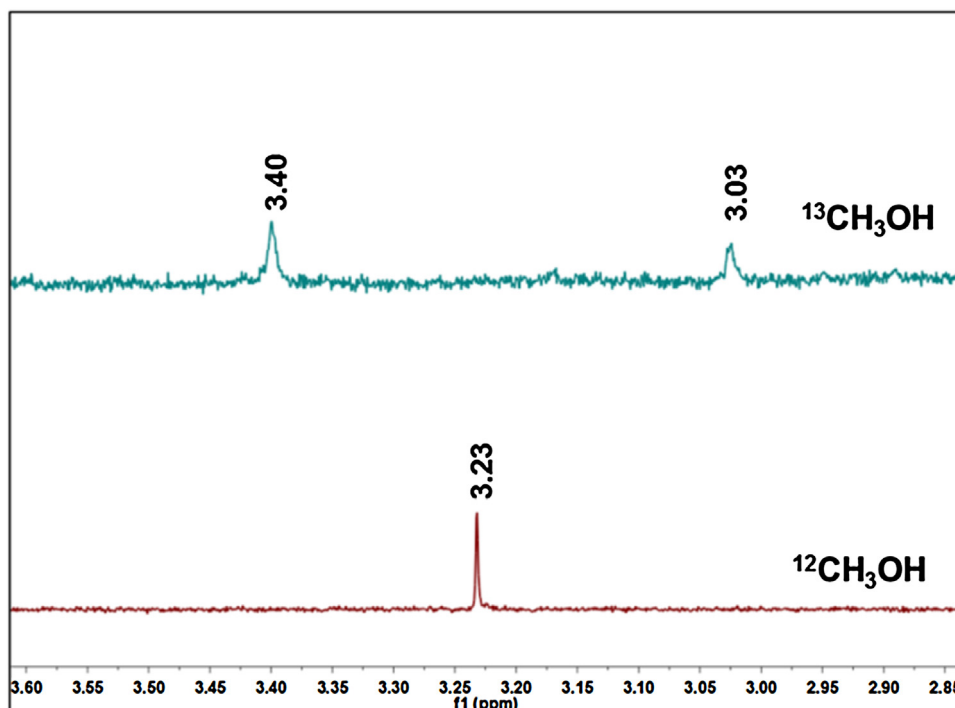**Fig. 9.** The formation rates of (a) CO and (b) H$_2$ for the four different photocathodes.

Fig. 10. ^{1}H NMR spectra of the methanol generated by photoelectrocatalytic reduction of $^{13}CO_2$ and $^{12}CO_2$ using dye-EDA-Pd@TiO$_2$ as the photocathode.

ent potentials are in the order of $-0.5 > -0.6 > -0.7 > -0.8$ V. When dye-EDA-Pd@TiO$_2$ electrode was utilized as the photocathode at -0.5 V, the highest Faradaic efficiency exceeded 1000%, which could be attributed to the synergistic effect of photoelectrons and counting electrons. For PEC cell with dye-R-Pd@TiO$_2$ photocathodes, as external bias potential increased (more negative) from -0.5 V to -0.8 V, the selectivity of carbon-based products was decreased gradually (Fig. 8b) because of the formation of H$_2$. Surprisingly, for each photocathode, the selectivity of methanol was nearly 100% when external potential is -0.5 V. As listed in Table S2, when the dye-DTA-Pd@TiO$_2$ electrode was served as the photocathode at -0.6 V, the selectivity of methanol was as high as 99.0%. Furthermore, when dye-MLM-Pd@TiO$_2$ was employed as the photocathode at -0.7 V, the formation rate of methanol was the highest (43.6 μM cm^{-2} h^{-1}). The total amount of products under more negative potential was notably larger than that under less negative potential. It can be found that the activities of dye-R-Pd@TiO$_2$ electrodes climbed up gradually when external potential ranged from -0.5 V to -0.8 V, agreeing with the formation rates of H$_2$ and CO (Fig. 9). The improved activities of multi-functionalized TiO$_2$ were presumably ascribed to the accelerated water splitting rate at more negative potential.

In addition, in order to contrast the CO$_2$ reduction activities of different photocathodes, four kinds of multi-functionalized TiO$_2$ electrodes were utilized in the PEC cells. As listed in Tables S1 and S2, when the bias potential was -0.7 V (*vs* SCE), the total products formation rates (TPFR) of dye-MLM-Pd@TiO$_2$, dye-CGD-Pd@TiO$_2$ and dye-DTA-Pd@TiO$_2$ photocathodes were 77.4, 68.7, and 47.3 μM cm^{-2} h^{-1}, respectively. However, the TPFR of dye-EDA-Pd@TiO$_2$ electrode was as high as 97.2 μM cm^{-2} h^{-1} and the Faradaic efficiency was 97% under the same conditions. Additionally, the control experiment using Pd@TiO$_2$ as the photocathode was carried out, and it showed low TPFR and Faradaic efficiency (Table S2).

Notably, some amounts of ethanol and acetone were generated in the new PEC cells, which required direct C—C coupling reaction. Herein, when the dye-EDA-Pd@TiO$_2$ electrode was used as
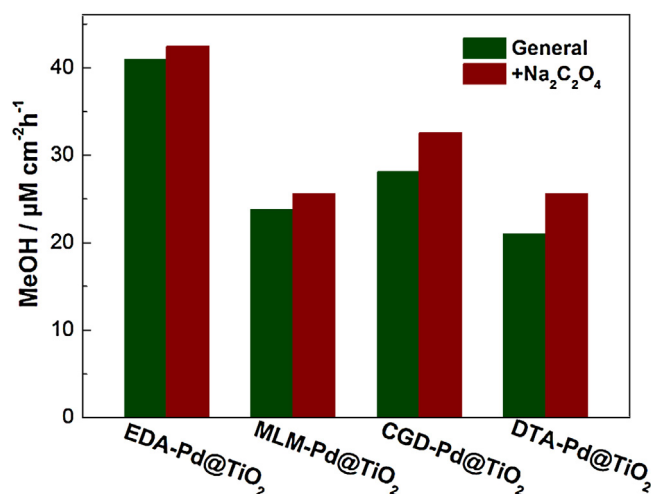

Fig. 11. The methanol formation rates of the four TiO$_2$ photocathodes when holes scavenger existed at -0.6 V *vs* SCE.

the photocathode, the formation rates of ethanol and acetone were as high as 14.0 and 0.7 μM cm^{-2} h^{-1}, respectively (Table S1). That can be attributed to the net-like structure feature on the surfaces of multi-functionalized TiO$_2$ (Fig. 1), which can provide abundant coordination sites to capture and activate CO$_2$. All these results indicated that the multi-functionalized TiO$_2$ electrodes could play vital roles in enhancing the reduction activity from CO$_2$ to chemical fuels. Furthermore, a blank experiment was conducted in Ar-saturated electrolyte under the same conditions, and no liquid or gas product was detected. The stability of EY was also considered. After 40 h irradiation under the optimal reaction conditions, the UV–vis absorption peaks of electrolyte were almost the same, suggesting the structure of dye was stable (Fig. S16) [25].
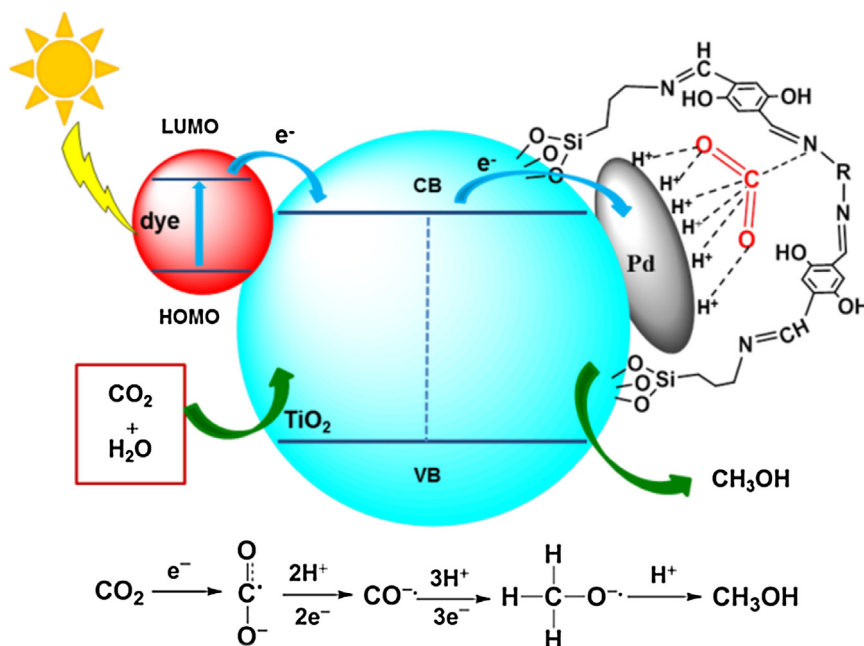
Fig. 12. Schematic mechanism for CO_2 reduction to methanol on the surface of multi-functionalized TiO_2 photocathodes.

3.4. $^{13}CO_2$ labeling experiments

In order to trace the carbon source of the main product CH_3OH, the $^{13}CO_2$ (Aldrich, 99%) isotopic labeling experiment was carried out in the PEC cell using dye-EDA-Pd@TiO$_2$ as the photocathode. After purging the whole system with Ar gas, $^{13}CO_2$ gas was bubbling into the well-sealed PEC device for 30 min. ^{1}H NMR and GC–MS techniques were utilized to analyze the liquid products and gas-phase products, respectively, after 8 h irradiation. As shown in Figs. 10 and S17, a doublet peak at 3.03 ppm and 3.40 ppm is attributed to the coupling of proton with the ^{13}C nucleus of $^{13}CH_3OH$. Meanwhile, both $^{13}CO_2$ (m/z 45) and ^{13}CO (m/z 29) were detected by GC–MS technique (Fig. S18). These results verify that the carbon atoms in CH_3OH and CO are indeed derived from CO_2.

3.5. Photoelectrocatalytic mechanism

Holes (h^+) trapping experiments using $Na_2C_2O_4$ as holes scavenger were performed to study the PEC CO_2 reduction mechanism [45]. It can be seen in Fig. 11 that, for R-Pd@TiO$_2$ photocathodes, the formation rates of methanol were improved from 3.6% to 21.8% when $Na_2C_2O_4$ existed. That implied that holes scavenger had positive effect on the CO_2 reduction in the new PEC cell. In brief, the electrons from holes scavenger can be injected into the TiO$_2$ holes, which could promote the separation efficiency of charge-hole. Accordingly, contrary to the oxidation of organic pollutants [27], the ability of CO_2 reduction was strengthened when holes scavenger existed.

On the basis of the experiment results, a possible mechanism was proposed for the PEC reduction of CO_2 to methanol (Fig. 12). Initially, the electrons in HOMO orbital of dye molecules could jump to the LUMO orbital under the irradiation of light [40,46]. Subsequently, the generated photoelectrons inject into the conduction band (CB) of TiO$_2$ and transfer to Pd nanoparticles. Then, the photoelectrons can be caught by protons on Pd nanoparticles to generate hydrogen atoms, or the photoelectrons could recombine with holes of TiO$_2$. The amines on the dye-R-Pd@TiO$_2$ surface could capture and activate dissolved CO_2 by forming $C\cdots N$ coordination bond [47]. When activated CO_2 receives an electron (photoelectron or electron

provided by workstation), the $CO_2^{-\bullet}$ radical forms [48]. The proton and hydrogen atom could attach to the oxygen in the $CO_2^{-\bullet}$ radical, resulting in the formations of carbon monoxide radical ($CO^{-\bullet}$) and H_2O. Moreover, the $CO^{-\bullet}$ radical could combine with three hydrogen atoms to form methoxyl radical ($CH_3O^{-\bullet}$) and CH_3OH is formed by combining $CH_3O^{-\bullet}$ with a proton. In addition, the $CO^{-\bullet}$ radical could convert into CO when one proton is obtained. On the other hand, the corresponding hydroxyl anions (OH^-) could move onto the Co-Pi/W:BiVO$_4$ film (counter electrode) and be oxidized to oxygen efficiently (Fig. S18) [49,50]. Alternatively, OH^- could be also oxidized to oxygen when the electrons transfer directly to the HOMO orbital of dyes rather than through external circuit. Thus, the Faradaic efficiencies of PEC cells might be exceeded 100%.

4. Conclusions

In summary, four different multi-functionalized TiO$_2$ electrodes modified with amine ligands, Pd nanoparticles and dye of EY were fabricated. The photoelectrocatalytic cells with multi-functionalized TiO$_2$ photocathodes can convert CO_2 to chemical fuels in water efficiently. In the new PEC cells, the adsorbed dyes could enlarge the light harvesting of TiO$_2$ and the Pd nanoparticles could accelerate the in-situ formation of hydrogen atoms. More importantly, amine ligands can capture and activate CO_2 dramatically. These improvements are beneficial to the coupling of water splitting and CO_2 reduction to generate carbon-based molecules. Methanol was the major liquid product, which was confirmed by $^{13}CO_2$ labeling experiment. The high Faradaic efficiency of new PEC cells could be ascribed to the synergistic effect of photocatalytic and electrocatalytic processes.

Appendix A. Supplementary data

Supplementary data associated with this article can be found, in the online version, at http://dx.doi.org/10.1016/j.apcatb.2016.12.039.

References

[1] T.R. Karl, K.E. Trenberth, Science 302 (2003) 1719–1723.
[2] N.M. Rezayee, C.A. Huff, M.S. Sanford, J. Am. Chem. Soc. 137 (2015) 1028–1031.
[3] M. Mikkelsen, M. Jorgensen, F.C. Krebs, Energy Environ. Sci. 3 (2010) 43–81.
[4] X. Jiang, F.L. Gou, F.J. Chen, H.W. Jing, Green Chem. 18 (2016) 3567–3576.
[5] M. Aresta, A. Dibenedetto, A. Angelini, Chem. Rev. 114 (2014) 1709–1742.
[6] W.G. Tu, Y. Zhou, Z.G. Zou, Adv. Mater. 26 (2014) 4607–4626.
[7] L. Liang, F.C. Lei, S. Gao, Y.F. Sun, X.C. Jiao, J. Wu, S. Qamar, Y. Xie, Angew. Chem. Int. Ed. 54 (2015) 13971–13974.
[8] A. Goeppert, M. Czaun, J.P. Jones, G.K.S. Prakash, G.A. Olah, Chem. Soc. Rev. 43 (2014) 7995–8048.
[9] X.X. Chang, T. Wang, J.L. Gong, Energy Environ. Sci. 9 (2016) 2177–2196.
[10] S. Lin, C.S. Diercks, Y.B. Zhang, N. Kornienko, E.M. Nichols, Y.B. Zhao, A.R. Paris, D. Kim, P.D. Yang, O.M. Yaghi, C.J. Chang, Science 349 (2015) 1208–1213.
[11] S. Zhang, P. Kang, S. Ubnoske, M.K. Brennaman, N. Song, R.L. House, J.T. Glass, T.J. Meyer, J. Am. Chem. Soc. 136 (2014) 7845–7848.
[12] M. Tahir, N.S. Amin, Appl. Catal. B: Environ. 142 (2013) 512–522.
[13] A. Fujishima, K. Honda, Nature 238 (1972) 37–38.
[14] T. Inoue, A. Fujishima, S. Konishi, K. Honda, Nature 277 (1979) 637–638.
[15] S.N. Habisreutinger, L. Schmidt-Mende, J.K. Stolarczyk, Angew. Chem. Int. Ed. 52 (2013) 7372–7408.
[16] Y. Ma, X.L. Wang, Y.S. Jia, X.B. Chen, H.X. Han, C. Li, Chem. Rev. 114 (2014) 9987–10043.
[17] P.D. Tran, L.H. Wong, J. Barber, J.S.C. Loo, Energy Environ. Sci. 5 (2012) 5902–5918.
[18] L.J. Liu, H.L. Zhao, J.M. Andino, Y. Li, ACS Catal. 2 (2012) 1817–1828.
[19] C.J. Wang, R.L. Thompson, P. Ohodnicki, J. Baltrus, C. Matranga, J. Mater. Chem. 21 (2011) 13452–13457.
[20] C.M. Li, G. Chen, J.X. Sun, H.J. Dong, Y. Wang, C. Lv, Appl. Catal. B: Environ. 160–161 (2014) 383–389.
[21] L. Cao, S. Sahu, P. Anilkumar, C.E. Bunker, J. Xu, K.A.S. Fernando, P. Wang, E.A. Guliants, K.N. Tackett, Y.P. Sun, J. Am. Chem. Soc. 133 (2011) 4754–4757.
[22] J. Zhang, Q. Xu, Z.C. Feng, M.J. Li, C. Li, Angew. Chem. Int. Ed. 47 (2008) 1766–1769.
[23] W.N. Wang, W.J. An, B. Ramalingam, S. Mukherjee, D.M. Niedzwiedzki, S. Gangopadhyay, P. Biswas, J. Am. Chem. Soc. 134 (2012) 11276–11281.
[24] C.M. Li, G. Chen, J.X. Sun, Y.J. Feng, J.J. Liu, H.J. Dong, Appl. Catal. B: Environ. 163 (2015) 415–423.
[25] X.J. Zhang, F. Han, B. Shi, S. Farsinezhad, G.P. Dechaine, K. Shankar, Angew. Chem. Int. Ed. 51 (2012) 12732–12735.
[26] Q.G. Zhai, S.J. Xie, W.Q. Fan, Q.H. Zhang, Y. Wang, W.P. Deng, Y. Wang, Angew. Chem. Int. Ed. 52 (2013) 5776–5779.
[27] Z. Zhu, Z.Y. Lu, D.D. Wang, X. Tang, Y.S. Yan, W.D. Shi, Y.S. Wang, N.L. Gao, X. Yao, H.J. Dong, Appl. Catal. B: Environ. 182 (2016) 115–122.
[28] N.M. Dimitrijevic, B.K. Vijayan, O.G. Poluektov, T. Rajh, K.A. Gray, H.Y. He, P. Zapol, J. Am. Chem. Soc. 133 (2011) 3964–3971.
[29] D. Finkelstein-Shapiro, S.H. Petrosko, N.M. Dimitrijevic, D. Gosztola, K.A. Gray, T. Rajh, P. Tarakeshwar, V. Mujica, J. Phys. Chem. Lett. 4 (2013) 475–479.
[30] X.F. Sun, Q.G. Zhu, X.C. Kang, H.Z. Liu, Q.L. Qian, Z.F. Zhang, B.X. Han, Angew. Chem. Int. Ed. 55 (2016) 6771–6775.
[31] T. Ohno, T. Higo, N. Murakami, H. Saito, Q.T. Zhang, Y. Yang, T. Tsubota, Appl. Catal. B: Environ. 152–153 (2014) 309–316.
[32] S. Zhang, P. Kang, T.J. Meyer, J. Am. Chem. Soc. 136 (2014) 1734–1737.
[33] C. Costentin, M. Robert, J.M. Saveant, Chem. Soc. Rev. 42 (2013) 2423–2436.
[34] D. Ren, Y.L. Deng, A.D. Handoko, C.S. Chen, S. Malkhandi, B.S. Yeo, ACS Catal. 5 (2015) 2814–2821.
[35] J.G. Yu, W.G. Wang, B. Cheng, B.L. Su, J. Phys. Chem. C 113 (2009) 6743–6750.
[36] T.T. Zhang, S.W. Cui, B. Yu, Z.L. Liu, D.A. Wang, Chem. Commun. 51 (2015) 16940–16943.
[37] S.P. Lin, S.Y. Huang, S.F. Chen, L.U. Vinzons, J.W. Ciou, P.J. Wong, ACS Appl. Mater. Interfaces 6 (2014) 12071–12082.
[38] W.G. Tu, Y. Zhou, H.J. Li, P. Li, Z.G. Zou, Nanoscale 7 (2015) 14232–14236.
[39] Y.H. Fu, D.R. Sun, Y.J. Chen, R.K. Huang, Z.X. Ding, X.Z. Fu, Z.H. Li, Angew. Chem. Int. Ed. 51 (2012) 3364–3367.
[40] F.L. Gou, X. Jiang, B. Li, H.W. Jing, Z.P. Zhu, ACS Appl. Mater. Interfaces 5 (2013) 12631–12637.
[41] Y.H. Qin, H.H. Yang, R.L. Lv, W.G. Wang, C.W. Wang, Electrochim. Acta 106 (2013) 372–377.
[42] G. Kumar, J.R. Blackburn, R.G. Albridge, W.E. Moddeman, M.M. Jones, Inorg. Chem. 11 (1972) 296–300.
[43] M.R. Jones, K.D. Osberg, R.J. Macfarlane, M.R. Langille, C.A. Mirkin, Chem. Rev. 111 (2011) 3736–3827.
[44] K.P. Kuhl, E.R. Cave, D.N. Abram, T.F. Jaramillo, Energy Environ. Sci. 5 (2012) 7050–7059.
[45] F.X. Zhang, Y. Pi, J. Cui, Y.L. Yang, X. Zhang, N.J. Guan, J. Phys. Chem. C 111 (2007) 3756–3761.
[46] F. Zhang, F. Shi, W. Ma, F. Gao, Y. Jiao, H. Li, J.C. Wang, X.Y. Shan, X.H. Lu, S. Meng, J. Phys. Chem. C 117 (2013) 14659–14666.
[47] M.L. Pinto, L. Mafra, J.M. Guil, J. Pires, J. Rocha, Chem. Mater. 23 (2011) 1387–1395.
[48] Q. Zhang, C.F. Lin, B.Y. Chen, T. Ouyang, C.T. Chang, Environ. Sci. Technol. 49 (2015) 2405–2417.
[49] J.A. Seabold, K.S. Choi, J. Am. Chem. Soc. 134 (2012) 2186–2192.
[50] S.K. Cho, H.S. Park, H.C. Lee, K.M. Nam, A.J. Bard, J. Phys. Chem. C 117 (2013) 23048–23056.